Hankel-based spectral method for quantitative acoustic microscopy

Lorena Leon, Jonathan Mamou, Denis Kouamé, Adrian Basarab

HANKEL-BASED SPECTRAL METHOD FOR QUANTITATIVE ACOUSTIC MICROSCOPY

Lorena Leon[1], *Jonathan Mamou*[2], *Denis Kouamé*[3], *and Adrian Basarab*[1]

[1]Univ Lyon, Université Claude Bernard Lyon 1, CNRS, Inserm, CREATIS UMR 5220, U1294, France
[2]Weill Cornell Medicine, Department of Radiology, New York, NY, USA
[3]IRIT, University of Toulouse, CNRS 5505, Université Paul Sabatier Toulouse 3, France

ABSTRACT

This work introduces a novel spectral-based framework for quantitative acoustic microscopy (QAM) applications. The proposed approach leverages Hankel (HK) matrix theory and an adaptive least squares method with an alternating direction method of multipliers. Simulation results and real-world experiments conducted with a 500-MHz QAM system demonstrate the robustness and efficiency of the proposed method. Comparative analysis with traditional autoregressive-based method shows a better accuracy in spectral and acoustic parameter estimation. Additionally, the HK-based method exhibits reduced variance in the presence of data corruptions, highlighting its potential for more reliable estimation.

Index Terms— Quantitative acoustic microscopy, spectral analysis, Hankel matrix, ADMM

1. INTRODUCTION

Quantitative acoustic microscopy (QAM) is an advanced imaging modality that leverages very high-frequency ultrasound, typically exceeding 200 MHz, to form high-resolution quantitative two-dimensional (2D) images of acoustical and mechanical properties of thin sections of soft biological tissues affixed to microscopy slides. These images offer resolutions finer than 8 μm, providing detailed information on properties such as the speed of sound, acoustic impedance, and acoustic attenuation [1]. This cutting-edge technology has been successfully employed in the examination of various soft biological tissues, including liver samples, lymph nodes, retina, and even living cells (see e.g., [2, 3]).

In the QAM data acquisition process, consisting of a 2D raster scan of the *ex vivo* sample with a high-frequency transducer, the received radio-frequency (RF) signal is typically composed of two leading reflections, originating from the interfaces between water (used as a coupling fluid between the transducer and the sample) and tissue, and tissue and glass slide. These reflections are time-shifted, frequency-attenuated, and amplitude-decayed versions of a reference reflection obtained from a water-glass interface. The challenge in QAM image formation lies in accurately decomposing the acquired RF signals into these two main reflections.

Time-domain methods have been proposed in QAM applications (e.g. [4]) and work well when the two signals are well-separated in time. In contrast, frequency-domain methods have proven valuable in scenarios where the reflections overlap in time, as demonstrated by the influential work of Hozumi et al. [5]. The current state of the art in QAM, as proposed by Rohrbach et al. [1], relies on an autoregressive (AR) frequency model and a spectral-based algorithm inspired by the classical Prony's method [6] and the annihilating filter [7]. This AR-based method has demonstrated clear superiority over previous approaches. However, its efficacy is constrained in situations involving thin tissue samples, high tissue speed of sound, small impedance contrast, or high tissue attenuation, thereby limiting the full potential of QAM.

Spectral analysis [8] is a broad field with numerous well-established methods, including popular algorithms like MUSIC [9] and ESPRIT [10]. In the spirit of [11], this paper introduces and investigates a novel spectral method within the QAM framework. Unlike AR modeling, this new algorithm addresses the spectral problem using the Hankel (HK) matrix theory and employs an alternating direction method of multipliers (ADMM). Our main goal is to enhance estimation accuracy and noise robustness in spectral estimation, leading to improved estimates of acoustic parameters and a reduction in the number of outliers produced by the aforementioned methods.

2. THEORETICAL BACKGROUND

2.1. Signal Model in Quantitative Acoustic Microscopy

In QAM applications, for a given spatial position of the transducer, the RF echo signal $h(t)$ is modeled as the sum of P weighted and delayed versions h_p of a reference signal h_0

$$h(t) = \sum_{p=1}^{P} h_p(t) = \sum_{p=1}^{P} a_p h_0^*(t - t_p), \tag{1}$$

where $*$ indicates an additional effect of frequency-dependent attenuation and $h_0(t - t_0)$ is obtained in practice from a region devoid of sample [1]. The parameters a_p and t_p in (1)

represent the amplitude decay and the shift in time of the pth signal h_p. Upon performing the discrete Fourier transform of an M-sized time-sampled version of (1) and dividing the Fourier coefficients of h by those of h_0, it is obtained a normalized spectrum

$$y_k = \sum_{p=1}^{P} a_p \underbrace{[\exp(2\pi\Delta f[-\beta_p - \mathrm{i}\Delta t_p])]}_{\lambda_p}{}^k = \sum_{p=1}^{P} a_p \lambda_p^k, \quad (2)$$

where the frequencies are given by $k\Delta f$, with $\Delta f = f_s/2M$ representing the step size for a sampling frequency f_s. The parameters β_p and $\Delta t_p = t_p - t_0$ are the frequency attenuation coefficient and the time delay of the pth signal. The normalization in (2) is well-defined where the Fourier coefficients of h_0 are nonzero. This is guaranteed in practice by restring frequencies between $k_{\text{min}}\Delta f$ and $k_{\text{max}}\Delta f$, which are determined by the -20-dB bandwidth of the transducer [1].

QAM principle consists of estimating $\boldsymbol{a} = (a_1, \ldots, a_P)$ and $\boldsymbol{\lambda} = (\lambda_1, \ldots, \lambda_P)$ using the truncated spectrum $\boldsymbol{y} = (y_{k_{\text{min}}}, \ldots, y_{k_{\text{max}}}) \in C^{2N+1}$, considering $2N = k_{\text{max}} - k_{\text{min}}$ without loss of generality. This involves solving a classical problem in spectral analysis [8]. Subsequently, the goal is to determine the spectral parameters associated with the two main signals in (1), which represent the echoes from the water-tissue and tissue-glass interfaces. The remaining $P-2$ signals account for potential multiple reflections, scattering, or noise. Without loss of generality, the two main reflections are denoted as h_{p_1} and h_{p_2}, with $p_1 \neq p_2$ and $\Delta t_{p_1} < \Delta t_{p_2}$. Finally, quantitative tissue properties can be directly computed using the estimates $\hat{a}_{p_1}$, $\hat{a}_{p_2}$, $\hat{\lambda}_{p_1}$, and $\hat{\lambda}_{p_2}$ along with the equations in (4).

In the following section, the approach for acoustic parameter estimation presented in [1] is recalled. It is based on an AR inverse model, and represents the state of the art, serving as a baseline for the new method proposed in this work.

2.2. AR-based Parameter Estimation

Preprocessing. Before applying the AR-based spectral decomposition method, in [1], a Cadzow filter [12] is used for denoising $\boldsymbol{y}$. This process involves iteratively reducing the rank of the Hankel matrix[1] $H(\boldsymbol{y})$. To do this, the singular value decomposition (SVD) $H(\boldsymbol{y}) = \boldsymbol{U}\boldsymbol{\Sigma}\boldsymbol{V}^\dagger$ is computed, where † denotes the conjugate transpose, $\boldsymbol{\Sigma}$ is a diagonal matrix containing singular values in descending order, and $\boldsymbol{U}$ and $\boldsymbol{V}$ are complex unitary matrices. Then, $H_P(\boldsymbol{y})$ is reconstructed by keeping only the P largest singular values of $\boldsymbol{\Sigma}$, i.e., $H_P(\boldsymbol{y}) = \boldsymbol{U}\boldsymbol{\Sigma}_P\boldsymbol{V}^\dagger$ where $[\boldsymbol{\Sigma}_P]_{ij} = [\boldsymbol{\Sigma}]_{ij}$ for $i, j \leq P$ and $[\boldsymbol{\Sigma}_P]_{ij} = 0$ otherwise. The denoised version $\boldsymbol{y}^D$ of $\boldsymbol{y}$ can be reconstructed by taking the average of all anti-diagonals of $H_P(\boldsymbol{y})$, i.e., $\boldsymbol{y}_n^D = \underset{i+j=n+1}{\text{mean}}([H_P(\boldsymbol{y})]_{ij})$. This procedure is repeated iteratively five times.

[1] *Hankel matrix* $\boldsymbol{A} = H(\boldsymbol{z})$ generated element-wise from a vector $\boldsymbol{z} = (z_1, \ldots, z_{2N+1})$, is defined as a matrix with constant anti-diagonals, such that $[\boldsymbol{A}]_{ij} = \boldsymbol{z}_{i+j-1}$.

The model order P must be predetermined, either set as a constant (e.g., $P \geq 2$), or during the first iteration of the Cadzow filter, P can be determined based on the number of singular values contributing more than 10% to the overall signal. The latter approach results in a more tailored representation of the underlying signal and is the strategy adopted in the present work.

AR-based estimation of $\boldsymbol{a}$ and $\boldsymbol{\lambda}$. The AR model assumes that y_k can be estimated using a linear combination of the P-previous Fourier coefficients

$$\boldsymbol{y}_{1+P\,:\,2N+1} = -\boldsymbol{R}\boldsymbol{s} + \boldsymbol{\epsilon}, \quad (3)$$

where $\boldsymbol{s}$ is the $P \times 1$ vector that gathers the AR coefficients and $\boldsymbol{\epsilon}$ is a $(2N+1-P)\times 1$ error vector. The matrix $\boldsymbol{R}$ has a size of $(2N+1-P)\times P$ with entries defined as $[\boldsymbol{R}]_{ij} = y_{k_{\text{min}}+P-i+j-1}$. The vector $\boldsymbol{s}$ is estimated from (3) using a least-squares (LS) approach, and $\boldsymbol{\lambda}$ is determined by the roots of polynomials formed by the elements of $\boldsymbol{s}$. The parameter $\boldsymbol{a}$ is obtained via an LS approach for solving $\boldsymbol{\Pi a} = \boldsymbol{y}$, where $\boldsymbol{\Pi}$ is a Vandermond-like matrix of size $(2N+1)\times P$, with entries defined as $[\boldsymbol{\Pi}]_{ij} = \lambda_j^i$, with $j = 1, \ldots, P$ and $i = k_{\text{min}}, \ldots, k_{\text{max}}$.

Acoustic parameter estimation. The P pulses are reconstructed using the estimates of $\boldsymbol{\lambda}$ and $\boldsymbol{a}$, and the amplitude of their envelopes (maximum of the Hilbert transform of the RF signals) is computed. The pulses corresponding to the two largest amplitudes are the desired components p_1 and p_2. The pulse p_1 from the water-tissue interface is the one with the shortest time of flight, since it occurs before the sample-glass-side interface. Finally, the speed of sound (c), the acoustic impedance (Z), the attenuation (α) and tissue thickness (d) can be computed as follows

$$\begin{aligned} c &= \frac{c_{\text{w}}\,\text{imag}(\ln\lambda_{p_1})}{\text{imag}(\ln\lambda_{p_1}) - \text{imag}(\ln\lambda_{p_2})},\ \alpha = \frac{-\,\text{real}(\ln\lambda_{p_2})}{4\pi d\Delta f}, \\ Z &= \frac{Z_{\text{w}}(1+\frac{a_{p_1}}{R_{\text{wg}}})}{1-\frac{a_{p_1}}{R_{\text{wg}}}}, \qquad d = \frac{c_{\text{w}}}{2}\frac{\text{imag}(\ln\lambda_{p_1})}{2\pi\Delta f}, \end{aligned} \quad (4)$$

where c_{w} and Z_{w} are the known speed of sound and acoustic impedance of water, and R_{wg} is the known pressure reflection coefficient between water and glass. In the context of QAM, estimates are considered outliers if they fall outside physically admissible ranges, specifically $c < 1500$, $c > 2200$, $Z < 1.48$, or $Z > 2.2$ [1].

3. PROPOSED HK-BASED PARAMETER ESTIMATION

The estimation accuracy of the acoustic parameters is affected by the estimation of the spectral parameters in (2). This can be particularly challenging in specific scenarios, e.g., for low signal-to-noise ratios, small values of d and small contrast between Z and Z_{w}. In this section, we introduce a novel approach for QAM image formation, considering that the Fourier coefficients in (2) are corrupted by additive Gaussian

noise. Our approach is inspired by the spectral method proposed in [11], which has not been adapted and tested within this context before, making it one of the key contributions of this work.

HK-based estimation of $\boldsymbol{a}$ and $\boldsymbol{\lambda}$. In our applications, k is equally spaced in $[k_{\text{min}}, k_{\text{max}}]$ and $\boldsymbol{y}$ is uniformly sampled. Consequently, the Kronecker's theorem[13, 14] for Hankel operators holds, implying that $\text{rank}(H(\boldsymbol{y})) = P$ if and only if $\boldsymbol{y}$ coincides at the sample points with $\boldsymbol{g}$ whose element corresponding to the kth frequency is defined as $g_k = \sum_{p=1}^{P} a_p \lambda_p^k$. Unlike the AR model, the spectral problem is not resolved directly in the parameter $\boldsymbol{a}, \boldsymbol{\lambda}$ space but in the space of the vectors that generate Hankel matrices of rank P. The corresponding optimization problem to find the best approximation of $\boldsymbol{y}$ in the l_2 sense read as

$$\begin{aligned} &\underset{\boldsymbol{A},\boldsymbol{g}}{\text{minimize}} \quad \frac{1}{2}||\boldsymbol{y}-\boldsymbol{g}||_2^2 + \mathcal{R}_P(\boldsymbol{A}) \\ &\text{subject to: } \boldsymbol{A} = H(\boldsymbol{g}), \end{aligned} \tag{5}$$

where $\mathcal{R}_P(\boldsymbol{A})$ is an indicator function, such that $\mathcal{R}_P(\boldsymbol{A}) = 0$ if $\text{rank}(\boldsymbol{A}) \leq P$ and infinity otherwise, and $||.||_2$ stands for l_2 vector norm. The augmented Lagrangian associated with (5) is

$$\begin{aligned} \mathcal{L}(\boldsymbol{A},\boldsymbol{g},\boldsymbol{\Lambda}) = &\mathcal{R}_P(\boldsymbol{A}) + \frac{1}{2}||\boldsymbol{y}-\boldsymbol{g}||_2^2 \\ &+ \langle \boldsymbol{\Lambda}, \boldsymbol{A} - H(\boldsymbol{g})\rangle_{\text{Re}} + \frac{\rho}{2}||\boldsymbol{A}-H(\boldsymbol{g})||_F^2, \end{aligned} \tag{6}$$

where $\boldsymbol{\Lambda}$ is the Lagrange multiplier matrix, ρ is a penalty coefficient to be chosen, $\langle \boldsymbol{A}, \boldsymbol{B}\rangle_{\text{Re}} = \text{real}(\text{tr}(\boldsymbol{A}\boldsymbol{B}^\dagger))$ denotes the scalar product between matrices $\boldsymbol{A}$ and $\boldsymbol{B}$ and $||\boldsymbol{A}||_F^2 = \langle \boldsymbol{A}, \boldsymbol{A}\rangle_{\text{Re}}$ denotes the Frobenius norm.

Problem (5)-(6) can be solved using a suitable ADMM method [15] with iterate steps $\boldsymbol{A}^{q+1} = \underset{\boldsymbol{A}}{\text{argmin}}\, \mathcal{L}(\boldsymbol{A}, \boldsymbol{g}^q, \boldsymbol{\Lambda}^q)$, $\boldsymbol{g}^{q+1} = \underset{\boldsymbol{g}}{\text{argmin}}\, \mathcal{L}(\boldsymbol{A}^{q+1}, \boldsymbol{g}, \boldsymbol{\Lambda}^q)$ and $\boldsymbol{\Lambda}^{q+1} = \boldsymbol{\Lambda}^q + \rho(\boldsymbol{A}^{q+1} - H(\boldsymbol{g}^{q+1}))$. Introducing the weights $\boldsymbol{w}_n = n$ if $n \leq N+1$ and $\boldsymbol{w}_n = N+2-n$ otherwise, and following the derivations in [11], the ADMM procedure is summarized in Algorithm 1.

Due to the term $\frac{\rho}{2}||\boldsymbol{A}-H(\boldsymbol{g})||_F^2$ in (6), one usually does not have $\hat{\boldsymbol{A}} = H(\hat{\boldsymbol{g}})$, where $\hat{\boldsymbol{A}}$ and $\hat{\boldsymbol{g}}$ are the estimates resulting from the ADMM algorithm. In other words, neither $\hat{\boldsymbol{g}}$ nor $\boldsymbol{y}^{\text{aprox}}$ obtained by averaging the anti-diagonals terms of $\hat{\boldsymbol{A}}$, i.e., $\boldsymbol{y}_n^{\text{aprox}} = \frac{1}{\boldsymbol{w}_n} \sum_{i+j=n+1} [\hat{\boldsymbol{A}}]_{ij}$, will be equal to a sum of exponential functions. Finally, it was observed that $\boldsymbol{y}^{\text{aprox}}$ is a more suitable solution than $\hat{\boldsymbol{g}}$. Assuming $\text{rank}(H(\boldsymbol{y}^{\text{aprox}})) = P$, $\boldsymbol{\lambda}$ can be obtained from the singular value decomposition $H(\boldsymbol{y}^{\text{aprox}}) = \boldsymbol{U}\boldsymbol{\Sigma}\boldsymbol{V}^\dagger$. Specifically, $\boldsymbol{\lambda}$ is the vector of eigenvalues of the matrix $(\boldsymbol{U}^l)^\dagger \boldsymbol{U}^f$, where $\boldsymbol{U}^f$ (resp. $\boldsymbol{U}^l$) denoted the matrix $\boldsymbol{U}$ of con-eigenvectors whose first row (resp. last row) has been dropped. Finally, the estimation of $\boldsymbol{a}$ and the acoustic parameter estimation remain as described in Section 2.2.

Algorithm 1: ADMM procedure

$\boldsymbol{g}_n^0 = \boldsymbol{y}$, $\boldsymbol{\Lambda}^0 = \boldsymbol{0}$
for $q = 1 : Q$ **do**
  $\boldsymbol{U}^q \boldsymbol{\Sigma}^q (\boldsymbol{V}^q)^\dagger = \text{svd}(H(\boldsymbol{g}^{q-1}) - \frac{1}{\rho}\boldsymbol{\Lambda}^{q-1})$
  $[\boldsymbol{\Sigma}_P^q]_{ij} = \begin{cases} [\boldsymbol{\Sigma}]_{ij}, & \text{if } i,j \leq P \\ 0, & \text{otherwise} \end{cases}$
  $\boldsymbol{A}^q = \boldsymbol{U}^q \boldsymbol{\Sigma}_P^q (\boldsymbol{V}^q)^\dagger$ *updating* $\boldsymbol{A}$
  for $n = 1 : 2N+1$ **do**
    $\boldsymbol{g}_n^q = \frac{1}{1+\rho \boldsymbol{w}_n}(\boldsymbol{y}_n + \sum_{i+j=n+1} [\rho \boldsymbol{A} + \boldsymbol{\Lambda}]_{ij})$
  end
  $\boldsymbol{\Lambda}^q = \boldsymbol{\Lambda}^{q-1} + \rho(\boldsymbol{A}^q - H(\boldsymbol{g}^q))$ *updating* $\boldsymbol{\Lambda}$
end
Result: $\hat{\boldsymbol{A}} = \boldsymbol{A}^Q, \hat{\boldsymbol{g}} = \boldsymbol{g}^Q$

4. EXPERIMENTS AND RESULTS

The performances of the AR-based ('AR') and the proposed HK-based ('HK') algorithms are compared on simulated and experimental 500-MHz QAM data. We also investigate the benefits of using the Cadzow filter in the proposed framework, considering an HK-based method ('HKw/oC') which processes the original spectrum, thus avoiding the preprocessing denoising step. For all algorithms, P was set using the criterion presented in Section 2.2. Additionally, for HK-based algorithms, we set the number of ADMM iterations to $Q = 200$ and the penalty coefficient to $\rho = 0.025$.

4.1. Simulations

To mimic a real-world scenario, we used a measured reference signal h_0 from our 500-MHz QAM system and set the acoustic parameters to experimentally relevant values based on [1]. Specifically, we used $d = 8\mu$m, $c = 1600$ m/s, $Z = 1.63$ MRayl and $\alpha = 10$ dB/MHz/cm, implying that $a_{p_1} = 0.0546$, $a_{p_2} = 0.9745$, $\lambda_{p_1} = 0.9112 + 0.4119$i and $\lambda_{p_2} = 0.9895 + 0.0315$i. We simulated RF signals following the model (1) for $P = 2$, $M = 300$ and perturbed them by a white Gaussian noise with a variance equal to σ^2, for $\sigma = 10^{(20\log_{10}((\xi(h_0)-\text{SNR})/20))}$ corresponding to a given signal-to-noise ratio (SNR). The symbol $\xi(h_0)$ represents the maximum of the Hilbert transform of h_0. In our study, we investigated the performance of AR, HK and HKw/oC methods on the estimation of spectral parameters (a_{p_1}, a_{p_2}, λ_{p_1}, λ_{p_2}) and acoustic parameters (d, c, Z, α) for SNR ranging from 40 to 100 dB, the typical SNR range in QAM. To assess performances, we calculated the mean error and standard deviation (STD) across 200 realizations after the outliers were removed.

Fig. 1 shows the performance results of the AR, HK and HKw/oC algorithms for the estimation of the spectral parameters in columns 1-3 and the acoustic parameters in columns 4-5. These results only considered the realizations where none

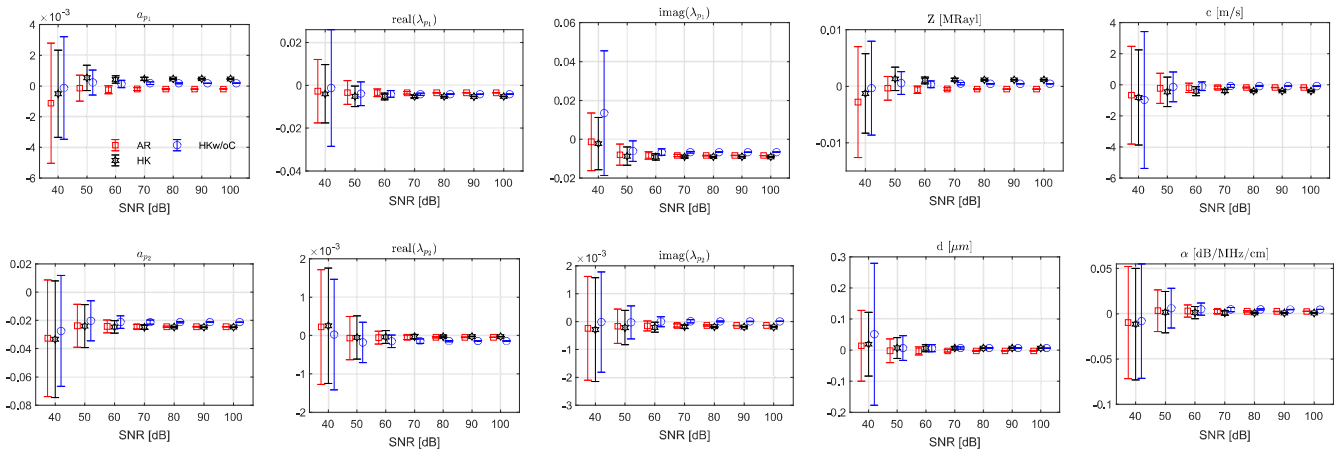

Fig. 1. Mean error and standard deviation results for AR (red), HK (black), and HKw/oC (blue) algorithms for different SNR values. Columns 1-3: Error in the estimated spectral parameters. Columns 4-5: Error in the estimated acoustic impedance ($Z = 1.63$ MRayl), speed of sound ($c = 1600$ m/s), attenuation coefficient ($\alpha = 10$ dB/MHz/cm), and thickness ($d = 8\mu$m).

of the algorithms returned outliers, which were only observed in the noisiest scenario (SNR $= 40$ dB). Specifically, at 40 dB, HK reported an 11% rate of outliers, lower than 13% and 31% obtained for AR and HKw/oC. Overall, all algorithms yield a mean error close to zero and small STD for high SNR values (i.e., SNR > 50 dB). Notably, at SNR $= 40$ dB, HK yielded a lower STD for the spectral parameters corresponding with the p_1 signal, implying the same behavior for Z and d.

4.2. *Ex vivo* experiments

The AR-based and HK-based algorithms were tested using experimental data obtained using the 500-MHz QAM system described in [16]. The data were collected from a 6-μm human lymph node section using a sampling frequency of 10 GHz. A 300-point RF signal was acquired at each spatial location using a 1-μm step size in both directions. A 0.140×0.135 micrometers (mm) spatial region of interest (ROI) was selected for analysis.

Fig. 2 (top) shows the estimated speed of sound maps from the analyzed ROI using the different algorithms: AR (left), HK (center), and HKw/oC (right). The outliers are marked in white. Notably, AR reported a larger rate of outliers ($\sim 27.8\%$) compared to HK ($\sim 19.6\%$) and HKw/oC ($\sim 20.3\%$). To mitigate outliers, standard QAM post-processing techniques were used; resulting images are shown in Fig. 2 (bottom), reporting $\sim 1.4\%$, $\sim 0.87\%$ and $\sim 0.89\%$ rate of outliers for AR, HK and HKw/oC, respectively. We can observe, mainly in the post-processing results, estimation differences between AR and HK-based algorithms. Finally, similar results were obtained for the remaining acoustic parameters of interest, although they are not presented here due to space limitations. Overall, the results of the HK-based methods are quite similar, implying that the use of the filter in the proposed approach might have a minimal impact on experiments and warrants further investigation.

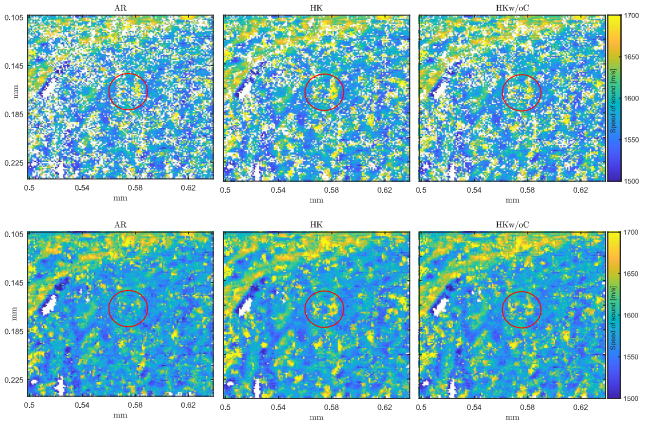

Fig. 2. Top: estimated c-maps, using AR (left), HK (center), and HKw/oC (right) algorithms. Bottom: post-processed estimated c-maps. A region illustrating the differences between the different estimators is shown in red.

5. CONCLUSIONS

We proposed a novel spectral method within the QAM framework. We conducted simulations to compare the performance of our approach with the traditional AR-based method. The results demonstrated that our method exhibits better performance in estimating both spectral and acoustic parameters in noisy scenarios. Furthermore, the proposed approach was tested in *ex vivo* experiments using our 500-MHz QAM system. It was found a lower percentage of outliers with our approach, emphasizing its robustness and reliability in practical applications.

6. COMPLIANCE WITH ETHICAL STANDARDS

The protocol (22-06024887) was approved by Weill Cornell Medicine Institutional Review board on August 2, 2023.

7. ACKNOWLEDGMENTS

We are grateful to the authors of [11] who have kindly provided us with the original code of their paper. This work was supported by NIH grant R01GM143388 (JM).

8. REFERENCES

[1] D. Rohrbach and J. Mamou, "Autoregressive signal processing applied to high-frequency acoustic microscopy of soft tissues," *IEEE Transactions on Ultrasonics, Ferroelectrics, and Frequency Control*, pp. 1–1, 2018.

[2] S. Irie, K. Inoue, K. Yoshida, J. Mamou, K. Kobayashi, H. Maruyama, and T. Yamaguchi, "Speed of sound in diseased liver observed by scanning acoustic microscopy with 80 MHz and 250 MHz," *The Journal of the Acoustical Society of America*, vol. 139, no. 1, pp. 512–519, Jan. 2016.

[3] J. A. Hildebrand, D. Rugar, R. N. Johnston, and C. F. Quate, "Acoustic microscopy of living cells.," *Proceedings of the National Academy of Sciences*, vol. 78, no. 3, pp. 1656–1660, Mar. 1981.

[4] G. A. D. Briggs, J. Wang, and R. Gungle, "Quantitative acoustic microscopy of individual living human cells," *Journal of Microscopy*, vol. 172, no. 1, pp. 3–12, Oct. 1993.

[5] N. Hozumi, R. Yamashita, C.-K Lee, M. Nagao, K. Kobayashi, Y. Saijo, M. Tanaka, N. Tanaka, and S. Ohtsuki, "Time–frequency analysis for pulse driven ultrasonic microscopy for biological tissue characterization," *Ultrasonics*, vol. 42, no. 1-9, pp. 717–722, Apr. 2004.

[6] G. R. Prony, "On the analysis of spectral lines by the method of least squares," *Royal Society of London Philosophical Transactions Series I*, vol. 85, pp. 373–518, 1795.

[7] K.-H. Jin, J.-C. Um, D.-H. Lee, J. Lee, S.-W. Park, and J.-C. Ye, "MRI artifact correction using sparse + low-rank decomposition of annihilating filter-based Hankel matrix," *Magnetic Resonance in Medicine*, vol. 78, no. 1, pp. 327–340, 2017.

[8] P. Stoica and R. L. Moses, *Introduction to Spectral Analysis*, Prentice Hall, 1997.

[9] R. Schmidt, "Multiple emitter location and signal parameter estimation," *IEEE Transactions on Antennas and Propagation*, vol. 34, no. 3, pp. 276–280, 1986.

[10] R. Roy and T. Kailath, "ESPRIT-estimation of signal parameters via rotational invariance techniques," *IEEE Transactions on Acoustics, Speech, and Signal Processing*, vol. 37, no. 7, pp. 984–995, 1989.

[11] F. Andersson, M. Carlsson, J.-Y. Tourneret, and H. Wendt, "A new frequency estimation method for equally and unequally spaced data," *IEEE T. Signal Proces.*, vol. 62, no. 21, pp. 5761–5774, Nov. 2014.

[12] J. A. Cadzow, "Signal enhancement-a composite property mapping algorithm," *IEEE Transactions on Acoustics, Speech, and Signal Processing*, vol. 36, no. 1, pp. 49–62, 1988.

[13] R. Rochberg, "Toeplitz and Hankel operators on the Paley-Wiener space," *Integral Equations and Operator Theory*, vol. 10, no. 2, pp. 187–235, Mar. 1987.

[14] F. Andersson, M. Carlsson, and M. V. de Hoop, "Sparse approximation of functions using sums of exponentials and AAK theory," *Journal of Approximation Theory*, vol. 163, no. 2, pp. 213–248, Feb. 2011.

[15] S. Boyd, N. Parikh, E. Chu, B. Peleato, and J. Eckstein, "Distributed optimization and statistical learning via the alternating direction method of multipliers," *Foundations and Trends® in Machine Learning*, vol. 3, no. 1, pp. 1–122, 2011.

[16] D. Rohrbach, A. Jakob, H. O. Lloyd, S. H. Tretbar, R. H. Silverman, and J. Mamou, "A novel quantitative 500-MHz acoustic microscopy system for ophthalmologic tissues," *IEEE Transactions on Biomedical Engineering*, vol. 64, no. 3, pp. 715–724, 2017.